

Article

# Refractive Bi-Conic Axicon (Volcone) for Polarization Conversion of Monochromatic Radiation

Sergey A. Degtyarev <sup>1,2,\*</sup> , Sergey V. Karpeev <sup>1,2</sup>, Nikolay A. Ivliev <sup>1,2</sup>, Yuriy S. Strelkov <sup>1,2</sup>, Vladimir V. Podlipnov <sup>1,2</sup>  and Svetlana N. Khonina <sup>1,2</sup> 

<sup>1</sup> IPSI RAS-Branch of the FSRC Crystallography and Photonics RAS, 443001 Samara, Russia; karp@ipsiras.ru (S.V.K.); ivlievn@gmail.com (N.A.I.); ghost\_strelkov@mail.ru (Y.S.S.); podlipnovvv@ya.ru (V.V.P.); khonina@ipsiras.ru (S.N.K.)

<sup>2</sup> Samara National Research University, 443086 Samara, Russia

\* Correspondence: sealek@gmail.com

**Abstract:** A new element is proposed for producing an azimuthally polarized beam with a vortex phase dependence. The element is formed by two conical surfaces in such a way that the optical element resembles a mountain with a crater on top, like a volcano (volcanic cone is volcone). The element in the form of a refractive bi-conic axicon is fabricated by diamond turning, in which an internal conical cavity is made. Polarization conversion in this optical element occurs on the inner surface due to the refraction of beams at the Brewster angle. The outer surface is used to collimate the converted beam, which significantly distinguishes the proposed element from previously proposed approaches. The paper describes a method for calculating the path of beams through a refractive bi-conic axicon, taking into account phase and polarization conversions. In the case of incident circularly polarized radiation, azimuthally polarized ring-shape beam radiation is generated at the output. The proposed element is experimentally made of polymethyl methacrylate on a CNC milling machine. The experiment demonstrates the effectiveness of the proposed element.

**Keywords:** geometric optics; bi-conic axicon; polarization; Fresnel coefficients; azimuthally polarized beam



**Citation:** Degtyarev, S.A.; Karpeev, S.V.; Ivliev, N.A.; Strelkov, Y.S.; Podlipnov, V.V.; Khonina, S.N. Refractive Bi-Conic Axicon (Volcone) for Polarization Conversion of Monochromatic Radiation. *Photonics* **2022**, *9*, 421. <https://doi.org/10.3390/photonics9060421>

Received: 13 May 2022

Accepted: 13 June 2022

Published: 16 June 2022

**Publisher's Note:** MDPI stays neutral with regard to jurisdictional claims in published maps and institutional affiliations.



**Copyright:** © 2022 by the authors. Licensee MDPI, Basel, Switzerland. This article is an open access article distributed under the terms and conditions of the Creative Commons Attribution (CC BY) license (<https://creativecommons.org/licenses/by/4.0/>).

## 1. Introduction

Considerable attention of researchers is being attracted by the possibility of forming inhomogeneously polarized beams, the structure of which can be very complex [1–12]. Such beams provide an additional degree of freedom in multiplexing and encoding optical information [13–16], as well as improved resolution in microscopy [17–19], enhanced capabilities in optical trapping and manipulation [20–22], and new effects in surface treatment and interaction with matter [23–30].

Structured laser beams have recently attracted much attention due to the promise of their interaction with azopolymers [31,32], which are photosensitive materials containing azofunctional groups. A distinctive feature of such materials is reversible photoisomerization and mass transfer induced by optical forces. The polarization anisotropy of azopolymer films makes it possible to use beams with radial and azimuthal polarizations both to analyze the molecular structure of an azopolymer [33] and to form a complex microrelief on its surface [34,35].

There are various approaches to the formation of inhomogeneously polarized beams, including interference methods [36–38], diffractive optical elements (DOEs) [39–41], spatial light modulators (SLMs) [42,43], subwavelength gratings and metasurfaces [44–47], as well as anisotropic crystals [48–53]. All methods have their advantages and disadvantages. SLMs convert only part of the transmitted light, thereby reducing the polarization extinction ratio. For a converter based on subwavelength gratings, the polarization contrast changes as a function of the angle of the polarization plane rotation. Although it can be compensated

by combining polarization and focusing elements [44,46], the technology of manufacturing subwavelength gratings for the visible wavelength range is quite complex.

The method for generating inhomogeneous polarizations by using refractive axicons with the Brewster angle is also well known [54–56]. The undoubted advantages of refractive axicons are high diffraction efficiency and low chromatic dispersion. However, the manufacture of refractive axicons is accompanied by certain difficulties, which are mainly due to the impossibility to fully control the conical surface quality [57,58]. Therefore, for polarization conversion, when the formation of a conical wavefront with a given angle of inclination to the optical axis is required, diffraction analogues of axicons are often used. This makes it possible to form cylindrical vector beams during multiple reflections in a stack of glass plates [59], as well as during the passage of polarizing films or crystals [60]. Moreover, diffractive axicons with a subwavelength period are used to form second-order cylindrically polarized beams [61]. In addition, axicons with a high numerical aperture are employed to enhance the longitudinal component of the electric field [62,63]. Refractive axicons cannot provide such a high numerical aperture due to the effect of total internal reflection [64]; however, multiple reflections of beams inside a refractive element can be used to implement other interesting transformations [65]. This possibility has led to various modifications of the classical cone prism [65]: narrow microaxicons or conical fiber optic probes [66,67], axicons with a spiral phase plate [68], logarithmic axicons [69,70], and axicons with nonlinear profiles [71,72], as well as “wrinkled” [73], twisted [74], and generalized [75,76] axicons.

In this paper, we propose a refractive bi-conic axicon for the transformation of a circular-polarized beams into an azimuthally polarized ring form vortex beam. The principle of operation is to use two conic surfaces: polarization conversion occurs on the inner surface due to the refraction of beams at the Brewster angle and the outer surface is used to collimate the converted beam. This is the essential difference between the proposed element and the previously proposed approaches.

Compared to subwavelength plates [61], bi-conic axicon has much less efficiency (~7% against ~25%) but is much simpler and cheaper to produce and does not need etching of diffractive relief at nanoscale. The energy efficiency of diffraction methods [38–40] and spatial light modulators [41–43] rarely exceeds 25%. Also, compared to diffractive relief or spatial light modulators, bi-axicon is more resistive to the high energy of laser beam, temperature, and external chemical and mechanical influences.

## 2. Theory and Simulation

### 2.1. Theoretical Description of the Method for Calculating the Beam Path

We propose a new refractive optical element for the generation of an azimuthally polarized beam with a vortex phase function. The element is formed by two conical surfaces in such a way that the inner conical cavity is made from the side of the pointed part of the truncated cone, so that a figure of rotation is formed, resembling a mountain with a crater at the top like a volcano. The central section of the element is shown in Figure 1a.

From bottom to top, a circularly polarized beam (green) is incident on the inner conical surface at the Brewster angle. The reflected part of the beam has azimuthal polarization. The second (outer) conical surface reflects the generated collimated beam forward. There is a technological offset  $\Delta$  from the outer radius of the bi-conic axicon. The offset is needed to ensure high quality of the working area of the second conical surface.

Let us present the derivation of the main formulae. Obviously, the incident and output beams must be collimated.

The proposed element is made of polymethyl methacrylate on a CNC milling machine.

During experimental studies, the bi-conic axicon was illuminated by a laser at a wavelength of 532 nm. The element material index for the given wavelength is:

$$n = 1.4958 \quad (1)$$

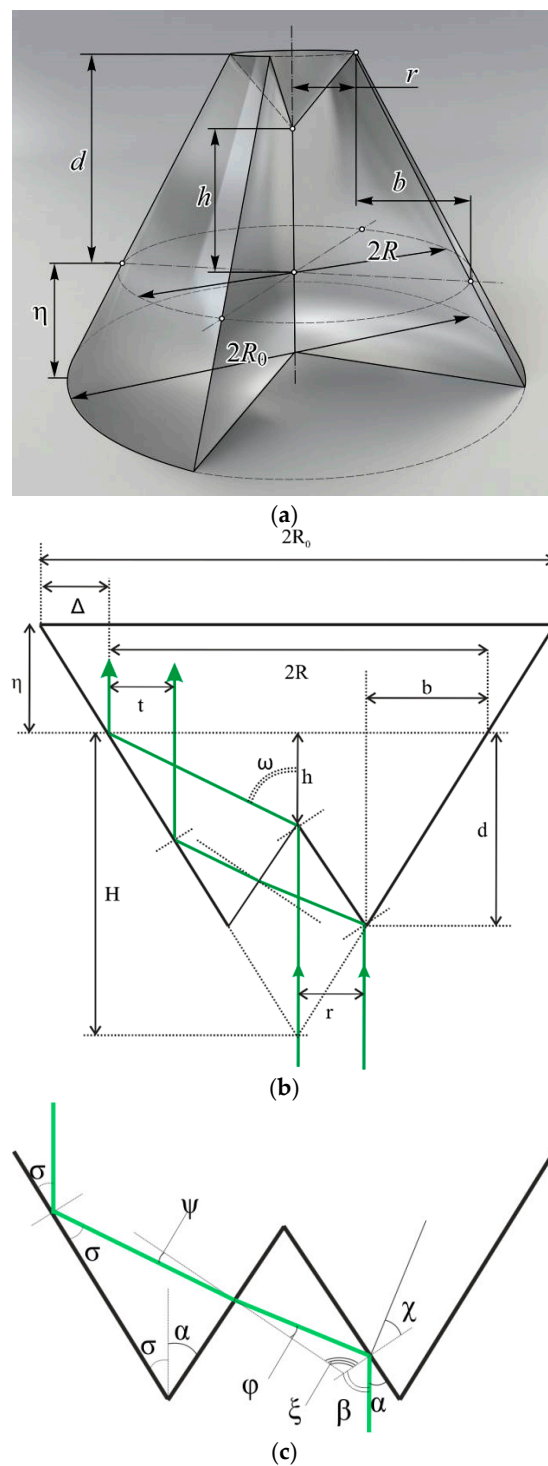


**Figure 1.** Schematic of a refractive bi-conic axicon: (a) 3D image of the volcone; (b) diagram indicating the dimensions of the axicon elements; (c) diagram indicating the angles of deflection of rays at refractions and reflections from the surfaces of the axicon.

The element was made from a cylinder with a radius  $R_0$ . The radius of the exit pupil of the axicon is denoted by the letter  $R$ .

The technological offset is expressed by the formula:

$$\Delta = R_0 - R \tag{2}$$

Then the offset of the edge of the working conical surface from the top edge of the element has the form:

$$\eta = \frac{\Delta}{\tan(\sigma)} \tag{3}$$

Letter designations of angles and sizes are introduced in Figure 1. Let us write down the basic formulae for the geometrical parameters of the axicon. The input beam is incident on the inner conical surface of the element at the Brewster angle

$$\beta = \arctan(n) \tag{4}$$

The beam reflected from the inner surface is s-polarized. Further, this beam again is incident on the inner surface of the axicon at an angle  $\varphi$ , is refracted at an angle  $\psi$ , and is incident at an angle  $\sigma$  on the outer conical surface of the element, where total internal reflection occurs. The reflected beam exits the element through the top face of the element parallel to the optical axis.

The angles during interaction with the axicon surfaces can be calculated using the formulae:

$$\alpha = \frac{\pi}{2} - \beta \tag{5}$$

$$\xi = \pi - 2\alpha \tag{6}$$

$$\varphi = \pi - \xi - \beta \tag{7}$$

$$\psi = \arcsin\left(\frac{\sin \varphi}{n}\right) \tag{8}$$

$$\chi = \alpha \tag{9}$$

$$\sigma = \frac{(\frac{\pi}{2} + \psi - \alpha)}{2} \tag{10}$$

$$\omega = \pi - 2\beta \tag{11}$$

$$h = \frac{R}{\tan(\omega)} \tag{12}$$

$$H = \frac{R}{\tan(\sigma)} \tag{13}$$

$$b = R - r \tag{14}$$

$$r = \frac{(H - h)}{\left(\frac{1}{\tan(\alpha)} + \frac{1}{\tan(\sigma)}\right)} \tag{15}$$

$$d = \frac{b}{\tan(\sigma)} \tag{16}$$

The element profile is defined by the polygon:

$$Volcone = \begin{bmatrix} 0 & 0 \\ d + \eta & b + \Delta \\ h + \eta & R + \Delta \\ d + \eta & r + R + \Delta \\ 0 & 2R_0 \end{bmatrix} \tag{17}$$

Let a plane-parallel beam with circular polarization is incident on the bi-conic axicon. The Jones vector of the incident beam is expressed as:

$$E = \begin{bmatrix} 1 \\ i \end{bmatrix} \tag{18}$$

When the initial beam is incident on the bi-conic axicon, a completely s-polarized beam is reflected. Thus, the volcone works as a polaroid that transmits polarization along the polar vector  $\varphi$ .

The Jones matrix of a linear polaroid is expressed as:

$$M = \begin{bmatrix} 1 & 0 \\ 0 & 0 \end{bmatrix} \tag{19}$$

If we take into account the spatial rotation of matrix (19) by the angle  $\varphi + \pi/2$ , then the Jones matrix will take the form [1,77]:

$$M_{volcone} = \begin{bmatrix} \cos(\varphi + \frac{\pi}{2}) & -\sin(\varphi + \frac{\pi}{2}) \\ \sin(\varphi + \frac{\pi}{2}) & \cos(\varphi + \frac{\pi}{2}) \end{bmatrix} \begin{bmatrix} 1 & 0 \\ 0 & 0 \end{bmatrix} \begin{bmatrix} \cos(\varphi + \frac{\pi}{2}) & \sin(\varphi + \frac{\pi}{2}) \\ -\sin(\varphi + \frac{\pi}{2}) & \cos(\varphi + \frac{\pi}{2}) \end{bmatrix} \tag{20}$$

$$= \begin{bmatrix} \sin^2(\varphi) & -\sin(\varphi)\cos(\varphi) \\ -\sin(\varphi)\cos(\varphi) & \cos^2(\varphi) \end{bmatrix}$$

After passing the incident beam through the bi-conic axicon, we obtain the following expression for the output field polarization:

$$E_{out} = \begin{bmatrix} \sin^2(\varphi) & -\sin(\varphi)\cos(\varphi) \\ -\sin(\varphi)\cos(\varphi) & \cos^2(\varphi) \end{bmatrix} \begin{bmatrix} 1 \\ i \end{bmatrix} \tag{21}$$

$$= \exp(i(\varphi - \frac{\pi}{2})) \begin{bmatrix} \sin(\varphi) \\ -\cos(\varphi) \end{bmatrix} = i \exp(i\varphi) \begin{bmatrix} -\sin(\varphi) \\ \cos(\varphi) \end{bmatrix}$$

It can be seen from Formula (21) that the output beam has azimuthal polarization with a first-order vortex phase.

2.2. Calculation of the Path of the Beams through a Volcone

The beam path in the element was calculated using software designed to take into account polarization ray tracing. We consider polarization state of each ray in Jones notation. Jones vector is transformed with Jones matrix which is automatically calculated for interaction of each ray with each surface. We calculate conversion efficiency as a ratio of passed integrated energy to incident integrated energy.

It is quite obvious that only a small part of the energy of the incident beam will form the output beam. The path of useful beams through a bi-conic axicon is shown in Figure 2.

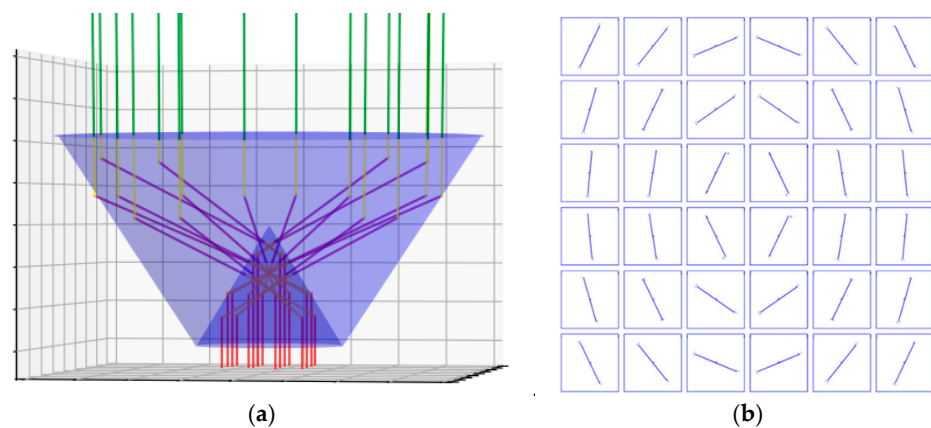


**Figure 2.** Path of the beams through a bi-conic axicon: (a) general appearance; (b) the polarization ellipse in the cross section of the output beam, calculated by the Formula (21).

In this case, the energy efficiency of the element is 6.6%.

The path of all the beams with a ray tracing depth of 5 is shown in Figure 3.

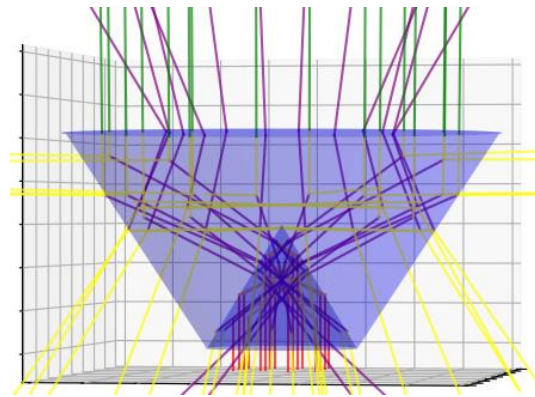


**Figure 3.** Path of the rays through a bi-conic axicon with a ray tracing depth of 5.

Figure 3 shows that, at a distance from the element, side beams are eliminated and a collimated azimuthally polarized beam is formed. Part of the energy is converted into a useful beam that propagates along the optical axis and is collimated. As can be seen in Figure 3, the remaining part of the energy is dissipated to the sides and at a short distance from the element completely leaves the zone of the useful beam. This fact is confirmed with experimental results.

We also considered the case of misalignment of the incident beam and the bi-conic axicon axis. The path of the beams through the bi-conic axicon for an incident beam inclination of  $5^\circ$  to the optical axis of the element is shown in Figure 4.

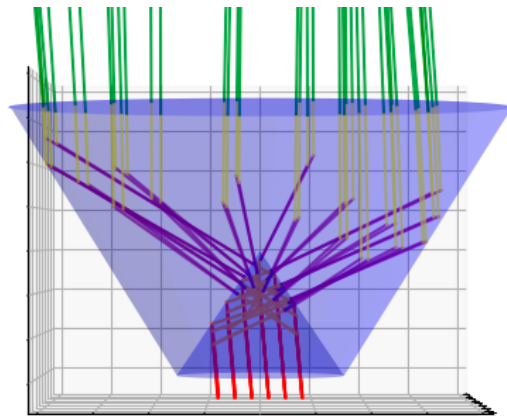


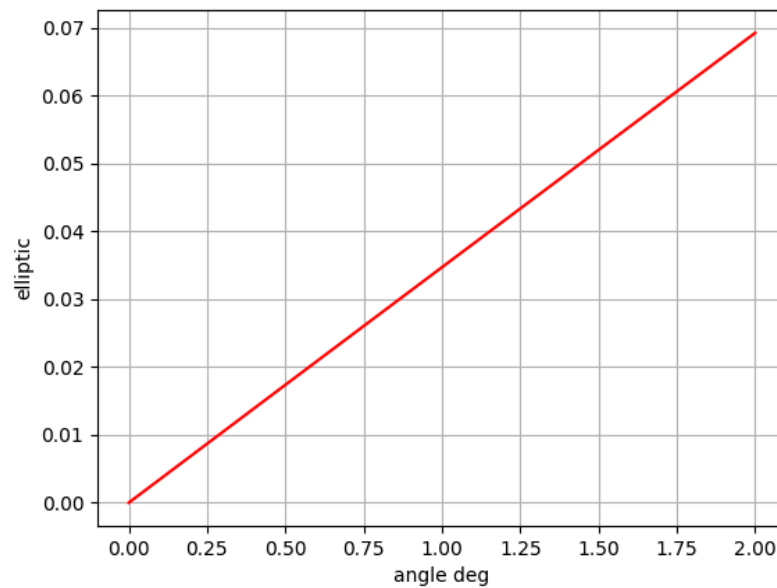
**Figure 4.** Path of the beams through a bi-conic axicon for an incident beam inclination of  $5^\circ$  to the optical axis of the element.

We conducted a study of the tolerance when the incident beam hits the icon of the conical axis at small angles. The incident beam tilt gives the resulting ray ellipticity. The dependence of ellipticity on the angle of inclination of the incident beam to the optical axis of the element is shown in Figure 5. We calculate ellipticity that is introduced when the incident beam falls into the element not exactly perpendicularly using proper accounting of the Jones vector for each ray.

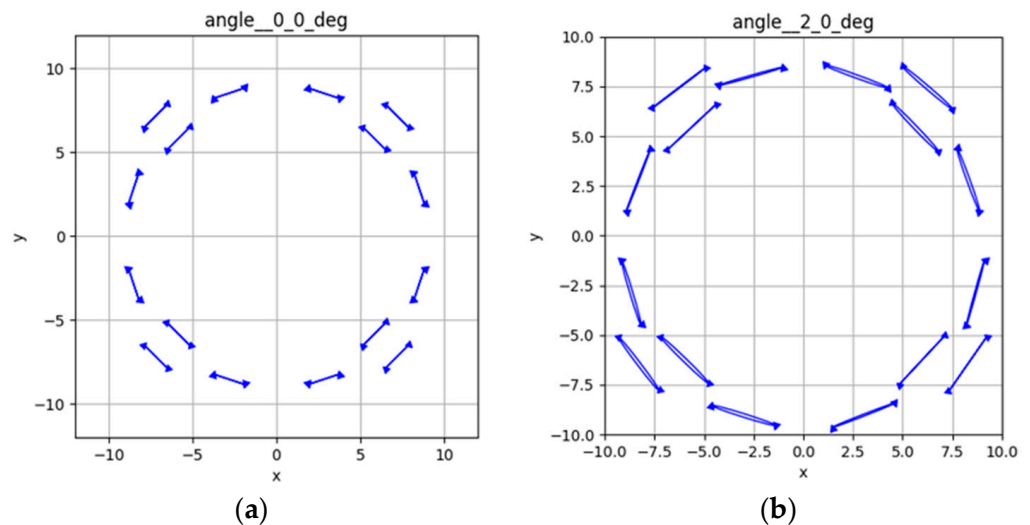
Figure 5 shows that the maximum ellipticity of one of the output rays depends almost linearly on the angle of displacement. This dependence shows the deviations of the polarization of the output beam with partially azimuthal polarization from an ideally polarized beam with ideal azimuthal polarization with an increase in the angle of inclination of the input beam with circular polarization.

Figure 6 shows exactly how the polarization of individual vectors changes when the angle of incidence of the initial beam deviates from the axis of the optical system. As can be seen, despite the appearance of ellipticity of the vectors that make up the azimuthal po-

larization, this ellipticity introduces less distortion into the overall polarization distribution and the average coefficient of ellipticity is significantly lower than the maximum.



**Figure 5.** Dependence of maximum ellipticity on the angle of inclination of the incident beam to the optical axis of the bi-conic axicon.



**Figure 6.** Image of the distribution of polarization vectors in the beam region: (a) in the absence of a deviation of the original beam; (b) with a deviation of 2 degrees.

### 3. Materials and Methods

The calculated axicon was made by lathe turning. The material used was PLEXIGLAS GS polymethyl methacrylate with a refractive index of 1.4958 for the 532 nm wavelength. The radius of the cutting edge of the tool used was 1 mm. The spindle speed during processing was equal to 1000 rpm, with the feed of 0.3 mm/rev. The specified turning regimes after the polishing made it possible to obtain an axicon surface of optical quality. The cylinder was not pre-treated. The appearance of the manufactured axicon is shown in Figure 7.



**Figure 7.** Appearance of the fabricated bi-conic axicon.

The schematic of the experimental setup for studying a laser beam formed by an axicon is shown in Figure 8. The initial linearly polarized laser beam of a solid-state laser with a wavelength of 532 nm was expanded and spatially filtered using a system consisting of a microobjective MO1 (20 $\times$ , NA = 0.4), a pinhole PH (aperture size 40  $\mu$ m), and a lens L1 (focal length 150 mm). A quarter-wave plate QWP was used to form circular polarization. A linear polarizer P was used to analyze the polarization state of the output radiation, which was directed at the translucent screen S. Then the image of the collimated azimuthally polarized beam was projected through the lens D2 onto the matrix of the video camera.

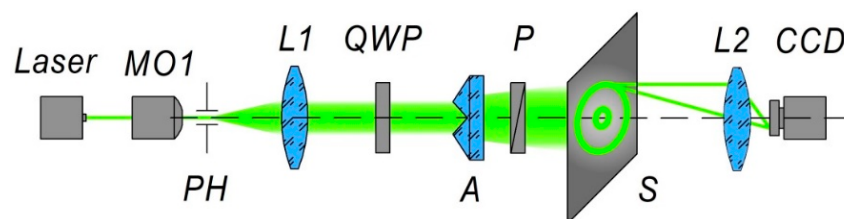


**Figure 8.** Schematic of the experimental setup.

The linear polarizer P was used to analyze the polarization state of the output radiation, which was directed at the translucent screen S. Then the image of the collimated azimuthally polarized beam was projected through the lens D2 onto the matrix of the video camera.

#### 4. Results and Discussion

As can be seen from the images of intensity distributions (Figure 9) at different screen distances from the bi-conic axicon, as a result of the passage of monochromatic circularly polarized radiation with a wavelength of 532 nm directed at the inner conical surface of the bi-conic axicon, the main part of the radiation is localized in two annular regions. These annular light distributions retain their structure when removed. From Figure 10 we can conclude that inner beam has an azimuthal polarization [5].

In this case, the inner ring is formed by a collimated azimuthally polarized laser beam with a small divergence. The remaining untransformed energy forms a strongly divergent outer ring and leaves the working area when removed.

The size of the image on the screen (Figure 9) corresponds to 160 mm. As can be seen from the images, the output beam (inner ring) with azimuthal polarization is collimated and its divergence does not exceed 6 mrad. The outer ring has a divergence of about 36 degrees that correspond to theoretical divergence angle of 34.9 degree. The inner ring has the theoretical radius  $R = 11$  mm and thickness  $t = 4$  mm. Experimentally measured meanings are approximately the same.

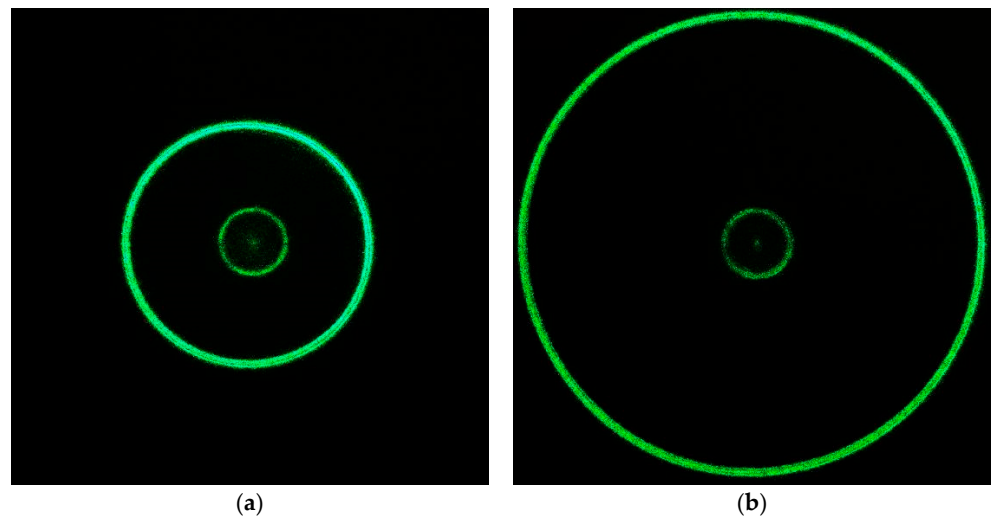


Figure 9. Light distribution at a distance: (a) 3 cm; (b) 8 cm.

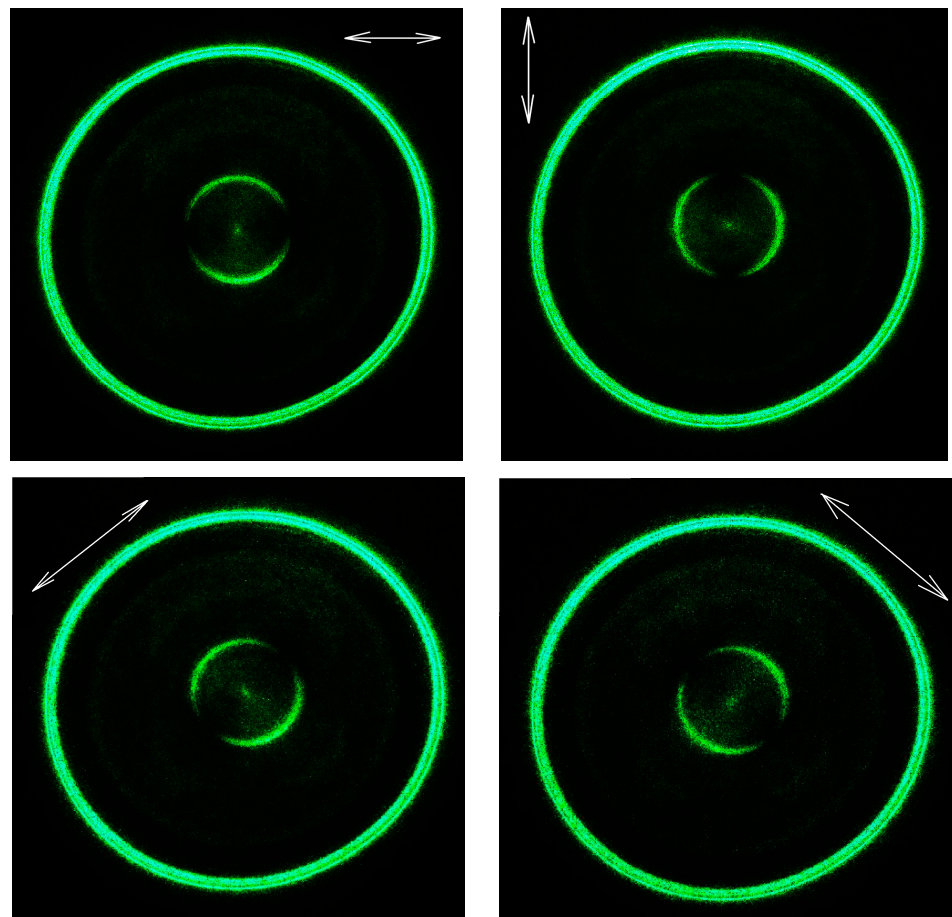


Figure 10. Results of the experiment. The intensity distributions that are obtained for different orientation of the analyzer-polarizer P.

This radiation is localized in the inner ring and the local area inside it. However, there is a non-zero intensity in the center caused by the presence of a vortex phase [78,79]. In the manufacture of the inner conical surface, it is quite difficult to perform turning and polishing in the area of the center of rotation without error. For the optical experiment, this area was closed to eliminate the effect of manufacturing inaccuracy. The geometric parameters of the conical surfaces, the ratio of the size of the inner cone and the outer

one, and the size of the overlap area in the center have an effect on the width and size of the rings in the area of the distribution of laser radiation intensity after passing the bi-conical axicon. In this experiment, we did not adhere to the goal of obtaining the necessary intensity distribution or the necessary dimensions of the annular intensity distribution of azimuthally polarized radiation.

Further, we investigate the transformation of the polarization of the input radiation from circular polarization to azimuthal. The images in Figure 10 show the intensity distributions that are obtained for different orientation of the analyzing polarizer. The white arrow shows the orientation of passing axis of analyzer-polarizer P.

The measured polarization extinction ratio from the images in the Figure 10 is 1:220 on average. The ratio of the energies of the outer ring with respect to the radiation concentrated in the ring with azimuthal polarization corresponds to 1:16, which corresponds to the efficiency modeling in Section 2.

However, a nonzero intensity is observed in the center, caused by the presence of a vortex phase [78,79]. The polarization state of this region corresponds to the circular polarization of the input beam. This feature is consistent with the calculation results (Formula (21)).

In the introduction, we mentioned that there are various approaches to the formation of inhomogeneously polarized beams. A feature of the proposed approach is to use both surfaces of the bi-conic axicon: polarization conversion occurs on the inner surface due to the refraction of beams at the Brewster angle and the outer surface is used to collimate the converted beam. This is the essential difference between the proposed element and the previously proposed approaches.

Note that the use of two surfaces for different transformations of the laser beam is only possible for a refractive element. The second (collimating) surface can be replaced by a diffractive element, but this will complicate the optical design and increase the cost.

Besides, the bi-conic axicon can be applied for high-power laser radiation. This makes it possible to compensate for the not very high efficiency of the polarization conversion.

## 5. Conclusions

We have presented simulation and experimental results of the proposed new refractive polarizing bi-conic axicon. The theoretical description and numerical investigation show that the suggested bi-conic axicon can produce an azimuthally-polarized ring-shape beam radiation at a given wavelength. Provided experiments verified the conceptual model and efficiency of proposed element. We have shown that the bi-axicon converts the input circularly polarized laser beam incident on the inner conical surface into an azimuthally polarized beam with a vortex phase dependence. We have demonstrated that the beam is also collimated by the outer surface of the axicon. Despite quite low efficiency (6.6%) of our element, it is sufficient for various microscopic researches [17–19], optical microtrapping [20–22], laser microablation, and microinteraction [23–32], as well as other applications where only a few percent of input laser energy or less is sufficient.

**Author Contributions:** Conceptualization, S.A.D. and S.V.K.; methodology, S.A.D. and Y.S.S.; software, S.A.D. and Y.S.S.; validation, S.A.D., Y.S.S., N.A.I. and S.N.K.; formal analysis, S.A.D. and S.N.K.; investigation, N.A.I. and V.V.P.; resources, N.A.I. and S.V.K.; data curation, Y.S.S.; writing—original draft preparation, S.A.D., N.A.I., S.V.K., V.V.P. and S.N.K.; writing—review and editing, V.V.P., S.V.K. and S.N.K.; visualization, V.V.P.; supervision, S.V.K. and S.N.K.; project administration, S.V.K.; funding acquisition, S.V.K. All authors have read and agreed to the published version of the manuscript.

**Funding:** This work was supported by the Russian Science Foundation (RSF), grant No. 22-12-00041.

**Institutional Review Board Statement:** Not applicable.

**Conflicts of Interest:** The authors declare no conflict of interest.

## References

1. Goldstein, D.H. *Polarized Light*; CRC Press: Boca Raton, FL, USA, 2003.
2. Freund, I. Polarization flowers. *Opt. Commun.* **2001**, *199*, 47–63. [[CrossRef](#)]
3. Maurer, C.; Jesacher, A.; Fürhapter, S.; Bernet, S.; RitschMarte, M. Tailoring of arbitrary optical vector beams. *New J. Phys.* **2007**, *9*, 78. [[CrossRef](#)]
4. Wang, X.L.; Li, Y.; Chen, J.; Guo, C.S.; Ding, J.; Wang, H.T. A new type of vector fields with hybrid states of polarization. *Opt. Express* **2010**, *18*, 10786–10795. [[CrossRef](#)] [[PubMed](#)]
5. Khonina, S.N.; Karpeev, S.V. Grating-based optical scheme for the universal generation of inhomogeneously polarized laser beams. *Appl. Opt.* **2010**, *49*, 1734–1738. [[CrossRef](#)] [[PubMed](#)]
6. Zhu, W.; She, W. Generation of tunable three-dimensional polarization in 4Pi focusing system. *Opt. Express* **2013**, *21*, 17265–17274. [[CrossRef](#)]
7. Rong, Z.-Y.; Han, Y.-J.; Wang, S.-Z.; Guo, C.-S. Generation of arbitrary vector beams with cascaded liquid crystal spatial light modulators. *Opt. Express* **2014**, *22*, 1636–1644. [[CrossRef](#)]
8. Liu, Z.; Liu, Y.; Ke, Y.; Liu, Y.; Shu, W.; Luo, H.; Wen, S. Generation of arbitrary vector vortex beams on hybrid-order Poincaré sphere. *Photon. Res.* **2017**, *5*, 15–21. [[CrossRef](#)]
9. Bauer, T.; Banzer, P.; Bouchard, F.; Orlov, S.; Marrucci, L.; Santamato, E.; Boyd, R.W.; Karimi, E.; Leuchs, G. Multi-twist polarization ribbon topologies in highly-confined optical fields. *New J. Phys.* **2019**, *21*, 053020. [[CrossRef](#)]
10. Khonina, S.N.; Ustinov, A.V.; Porfirev, A.P. Vector Lissajous laser beams. *Opt. Lett.* **2020**, *45*, 4112–4115. [[CrossRef](#)]
11. Zhong, R.Y.; Zhu, Z.H.; Wu, H.J.; Rosales-Guzmán, C.; Song, S.W.; Shi, B.S. Gouy phase-mediated propagation variations and revivals of transverse structure in vectorially structured light. *Phys. Rev. A* **2021**, *103*, 053520. [[CrossRef](#)]
12. Khonina, S.N.; Porfirev, A.P. Harnessing of inhomogeneously polarized Hermite–Gaussian vector beams to manage the 3D spin angular momentum density distribution. *Nanophotonics* **2022**, *11*, 697–712. [[CrossRef](#)]
13. Milione, G.; Nguyen, T.A.; Leach, J.; Nolan, D.A.; Alfano, R.R. Using the nonseparability of vector beams to encode information for optical communication. *Opt. Lett.* **2015**, *40*, 4887–4890. [[CrossRef](#)] [[PubMed](#)]
14. Akent'ev, A.S.; Sadovnikov, M.A.; Sokolov, A.L.; Simonov, G.V. Polarization analysis of the beam-steering device of quantum optical systems. *Opt. Spectrosc.* **2017**, *122*, 1008–1014. [[CrossRef](#)]
15. Ndagano, B.; Nape, I.; Cox, M.A.; Rosales-Guzman, C.; Forbes, A. Creation and detection of vector vortex modes for classical and quantum communication. *J. Lightwave Technol.* **2018**, *36*, 292–301. [[CrossRef](#)]
16. Karpeev, S.V.; Podlipnov, V.V.; Khonina, S.N.; Ivliev, N.A.; Ganchevskaya, S.V. Free-space transmission and detection of variously polarized near-IR beams using standard communication systems with embedded singular phase structures. *Sensors* **2022**, *22*, 890–907. [[CrossRef](#)]
17. Oron, D.; Tal, E.; Silberberg, Y. Depth-resolved multiphoton polarization microscopy by third-harmonic generation. *Opt. Lett.* **2003**, *28*, 2315–2317. [[CrossRef](#)]
18. Serrels, K.; Ramsay, E.; Warburton, R.; Reid, D. Nanoscale optical microscopy in the vectorial focusing regime. *Nat. Photonics* **2008**, *2*, 311–314. [[CrossRef](#)]
19. Kenny, F.; Lara, D.; Rodríguez-Herrera, O.; Dainty, C. Complete polarization and phase control for focus-shaping in high-NA microscopy. *Opt. Express* **2012**, *20*, 14015–14029. [[CrossRef](#)]
20. Skelton, S.; Sergides, M.; Saija, R.; Iati, M.; Marago, O.; Jones, P. Trapping volume control in optical tweezers using cylindrical vector beams. *Opt. Lett.* **2013**, *38*, 28–30. [[CrossRef](#)]
21. Otte, E.; Denz, C. Optical trapping gets structure: Structured light for advanced optical manipulation. *Appl. Phys. Rev.* **2020**, *7*, 041308. [[CrossRef](#)]
22. Yang, Y.; Ren, Y.; Chen, M.; Arita, Y.; Rosales-Guzmán, C. Optical trapping with structured light: A review. *Adv. Photonics* **2021**, *3*, 034001. [[CrossRef](#)]
23. Gorodetski, Y.; Niv, A.; Kleiner, V.; Hasman, E. Observation of the spin-based plasmonic effect in nanoscale structures. *Phys. Rev. Lett.* **2008**, *101*, 043903. [[CrossRef](#)] [[PubMed](#)]
24. Beresna, M.; Gecevičius, M.; Kazansky, P.G.; Gertus, T. Radially polarized optical vortex converter created by femtosecond laser nanostructuring of glass. *Appl. Phys. Lett.* **2011**, *98*, 201101. [[CrossRef](#)]
25. Müller, T.; Schumann, C.; Kraegeloh, A. STED Microscopy and its applications: New insights into cellular processes on the nanoscale. *Chemphyschem* **2012**, *13*, 1986–2000. [[CrossRef](#)] [[PubMed](#)]
26. Khonina, S.N.; Golub, I. How low can STED go? Comparison of different write-erase beam combinations for stimulated emission depletion microscopy. *J. Opt. Soc. Am. A* **2012**, *29*, 2242–2246. [[CrossRef](#)]
27. Varin, C.; Payeur, S.; Marceau, V.; Fourmaux, S.; April, A.; Schmidt, B.; Fortin, P.-L.; Thire, N.; Brabec, T.; Legare, F.; et al. Direct electron acceleration with radially polarized laser beams. *Appl. Sci.* **2013**, *3*, 70–93. [[CrossRef](#)]
28. Ni, J.; Wang, C.; Zhang, C.; Hu, Y.; Yang, L.; Lao, Z.; Chu, J. Three-dimensional chiral microstructures fabricated by structured optical vortices in isotropic material. *Light Sci. Appl.* **2017**, *6*, e17011. [[CrossRef](#)] [[PubMed](#)]
29. Syubaev, S.A.; Zhizhchenko, A.Y.; Pavlov, D.V.; Gurbatov, S.O.; Pustovalov, E.V.; Porfirev, A.P.; Khonina, S.N.; Kulinich, S.A.; Rayappan, J.B.B.; Kudryashov, S.I.; et al. Plasmonic nanolenses produced by cylindrical vector beam printing for sensing applications. *Sci. Rep.* **2019**, *9*, 19750. [[CrossRef](#)]

30. Porfirev, A.P.; Khonina, S.N.; Meshalkin, A.; Ivliev, N.A.; Achimova, E.; Abashkin, V.; Prisar, A.; Podlipnov, V.V. Two-step maskless fabrication of compound fork-shaped gratings in nanomultilayer structures based on chalcogenide glasses. *Opt. Lett.* **2021**, *46*, 3037–3040. [[CrossRef](#)]
31. Masuda, K.; Nakano, S.; Barada, D.; Kumakura, M.; Miyamoto, K.; Omatsu, T. Azo-polymer film twisted to form a helical surface relief by illumination with a circularly polarized Gaussian beam. *Opt. Express* **2017**, *25*, 12499–12507. [[CrossRef](#)]
32. Khonina, S.N.; Ustinov, A.V.; Volotovskiy, S.G.; Ivliev, N.A.; Podlipnov, V.V. Influence of optical forces induced by paraxial vortex Gaussian beams on the formation of a microrelief on carbazole-containing azopolymer films. *Appl. Opt.* **2020**, *59*, 9185–9194. [[CrossRef](#)] [[PubMed](#)]
33. Kharintsev, S.S.; Fishman, A.I.; Kazarian, S.G.; Salakhov, M.K. Polarization of near-field light induced with a plasmonic nanoantenna. *Phys. Rev. B* **2015**, *92*, 115113. [[CrossRef](#)]
34. Masuda, K.; Shinozaki, R.; Shiraishi, A.; Ichijo, M.; Yamane, K.; Miyamoto, K.; Omatsu, T. Picosecond optical vortex-induced chiral surface relief in an azo-polymer film. *J. Nanophoton.* **2020**, *14*, 016012. [[CrossRef](#)]
35. Ferrer-Garcia, M.F.; Alvandi, Y.; Zhang, Y.; Karimi, E. Theoretical analysis on spatially structured beam induced mass transport in azo-polymer films. *Opt. Express* **2020**, *28*, 19954–19965. [[CrossRef](#)] [[PubMed](#)]
36. Tidwell, S.C.; Ford, D.H.; Kimura, W.D. Generating radially polarized beams interferometrically. *Appl. Opt.* **1990**, *29*, 2234–2239. [[CrossRef](#)] [[PubMed](#)]
37. Passilly, N.; de Saint, D.R.; Ait-Ameur, K.; Treussart, F.; Hierle, R.; Roch, J.-F. Simple interferometric technique for generation of a radially polarized light beam. *J. Opt. Soc. Am. A* **2005**, *22*, 984–991. [[CrossRef](#)]
38. Liu, S.; Li, P.; Peng, T.; Zhao, J. Generation of arbitrary spatially variant polarization beams with a trapezoid Sagnac interferometer. *Opt. Express* **2012**, *20*, 21715–21721. [[CrossRef](#)]
39. Khonina, S.N.; Karpeev, S.V. Generating inhomogeneously polarized higher-order laser beams by use of diffractive optical elements. *J. Opt. Soc. Am. A* **2011**, *28*, 2115–2123. [[CrossRef](#)]
40. Sokolov, A.L.; Murashkin, V.V. Diffraction polarization optical elements with radial symmetry. *Opt. Spectrosc.* **2011**, *111*, 859–865. [[CrossRef](#)]
41. Porfirev, A.P.; Ustinov, A.V.; Khonina, S.N. Polarization conversion when focusing cylindrically polarized vortex beams. *Sci. Rep.* **2016**, *6*, 6. [[CrossRef](#)]
42. Moreno, I.; Davis, J.A.; Hernandez, T.M.; Cottrell, D.M.; Sand, D. Complete polarization control of light from a liquid crystal spatial light modulator. *Opt. Express* **2012**, *20*, 364–376. [[CrossRef](#)] [[PubMed](#)]
43. Karpeev, S.V.; Podlipnov, V.V.; Algubili, A.M. An interference scheme for generating inhomogeneously polarized laser radiation using a spatial light modulator. *Comput. Opt.* **2020**, *44*, 214–218. [[CrossRef](#)]
44. Bomzon, Z.; Biener, G.; Kleiner, V.; Hasman, E. Radially and azimuthally polarized beams generated by space-variant dielectric subwavelength gratings. *Opt. Lett.* **2002**, *27*, 285–287. [[CrossRef](#)] [[PubMed](#)]
45. Lerman, G.M.; Levy, U. Generation of a radially polarized light beam using space-variant subwavelength gratings at 1064 nm. *Opt. Lett.* **2008**, *33*, 2782–2784. [[CrossRef](#)]
46. Rubin, N.A.; Zaidi, A.; Juhl, M.; Li, R.P.; Mueller, J.B.; Devlin, R.C.; Leosson, K.; Capasso, F. Polarization state generation and measurement with a single metasurface. *Opt. Express* **2018**, *26*, 21455–21478. [[CrossRef](#)]
47. Khonina, S.N.; Degtyarev, S.A.; Ustinov, A.V.; Porfirev, A.P. Metalenses for the generation of vector Lissajous beams with a complex Poynting vector density. *Opt. Express* **2021**, *29*, 18651–18662. [[CrossRef](#)]
48. Machavariani, G.; Lumer, Y.; Moshe, I.; Meir, A.; Jackel, S.; Davidson, N. Birefringence-induced bifocusing for selection of radially or azimuthally polarized laser modes. *Appl. Opt.* **2007**, *46*, 3304–3310. [[CrossRef](#)]
49. Karpeev, S.V.; Podlipnov, V.V.; Khonina, S.N.; Parandin, V.D.; Tukmakov, K.N. Anisotropic diffractive optical element for generating hybrid-polarized beams. *Opt. Eng.* **2019**, *58*, 082402.
50. Loussert, C.; Brasselet, E. Efficient scalar and vectorial singular beam shaping using homogeneous anisotropic media. *Opt. Lett.* **2010**, *35*, 7–9. [[CrossRef](#)]
51. Fadeyeva, T.A.; Shvedov, V.G.; Izdebskaya, Y.V.; Volyar, A.V.; Brasselet, E.; Neshev, D.N.; Desyatnikov, A.S.; Krolikowski, W.; Kivshar, Y.S. Spatially engineered polarization states and optical vortices in uniaxial crystals. *Opt. Express* **2010**, *18*, 10848–10863.
52. Khonina, S.N.; Karpeev, S.V.; Parandin, V.D.; Morozov, A.A. Polarization conversion under focusing of vortex laser beams along the axis of anisotropic crystals. *Phys. Lett. A* **2017**, *381*, 2444–2455. [[CrossRef](#)]
53. Khonina, S.N.; Porfirev, A.P.; Kazanskiy, N.L. Variable transformation of singular cylindrical vector beams using anisotropic crystals. *Sci. Rep.* **2020**, *10*, 5590. [[CrossRef](#)] [[PubMed](#)]
54. Tovar, A.A. Production and propagation of cylindrically polarized Laguerre–Gaussian laser beams. *J. Opt. Soc. Am. A* **1998**, *15*, 2705–2711. [[CrossRef](#)]
55. Kozawa, Y.; Sato, S. Generation of a radially polarized laser beam by use of a conical Brewster prism. *Opt. Lett.* **2005**, *30*, 3063–3065. [[CrossRef](#)] [[PubMed](#)]
56. Radwell, N.; Hawley, R.D.; Gotte, J.B.; Franke-Arnold, S. Achromatic vector vortex beams from a glass cone. *Nat. Commun.* **2016**, *7*, 10654. [[CrossRef](#)]
57. Zhang, Y.; Zeng, A.; Wang, Y.; Huang, H. A method for measuring the base angle of axicon lens based on chromatic dispersion. *Opt. Commun.* **2015**, *346*, 69–73. [[CrossRef](#)]

58. Wei, Z.; Yuan, Q.; Ma, X.; Hu, J.; Zeng, A.; Huang, H. Measurement of base angle of an axicon lens based on autocollimation optical path. *Opt. Commun.* **2019**, *434*, 23–27. [[CrossRef](#)]
59. Skidanov, R.V.; Morozov, A.A. Diffractive optical elements for forming radially polarized light, based on the use stack of Stoletov. *Comput. Opt.* **2014**, *38*, 614–618. [[CrossRef](#)]
60. Karpeev, S.V.; Parandin, V.D.; Khonina, S.N. Generation of a controlled double-ring-shaped radially polarized spiral laser beam using a combination of a binary axicon with an interference polarizer. *J. Opt.* **2017**, *19*, 055701. [[CrossRef](#)]
61. Khonina, S.N.; Tukmakov, K.N.; Degtyarev, S.A.; Reshetnikov, A.S.; Pavelyev, V.S.; Knyazev, B.A.; Choporova, Y.Y. Design, fabrication and investigation of a subwavelength axicon for terahertz beam polarization transforming. *Comput. Opt.* **2019**, *43*, 756–764. [[CrossRef](#)]
62. Urbach, H.P.; Pereira, S.F. Field in Focus with a Maximum Longitudinal Electric Component. *Phys. Rev. Lett.* **2008**, *100*, 123904. [[CrossRef](#)] [[PubMed](#)]
63. Khonina, S.N.; Savelyev, D.A. High-aperture binary axicons for the formation of the longitudinal electric field component on the optical axis for linear and circular polarizations of the illuminating beam. *J. Exp. Theor. Phys.* **2013**, *117*, 623–630. [[CrossRef](#)]
64. Ustinov, A.V.; Khonina, S.N. Calculation of complex transmission function of refractive axicons. *Comput. Opt.* **2011**, *35*, 480–490.
65. Khonina, S.N.; Degtyarev, S.A.; Savelyev, D.A.; Ustinov, A.V. Focused, evanescent, hollow, and collimated beams formed by microaxicons with different conical angles. *Opt. Express* **2017**, *25*, 19052–19064. [[CrossRef](#)] [[PubMed](#)]
66. Yu, Y.-J.; Noh, H.; Hong, M.-H.; Noh, H.-R.; Arakawa, Y.; Jhe, W. Focusing characteristics of optical fiber axicon microlens for near-field spectroscopy: Dependence of tip apex angle. *Opt. Commun.* **2006**, *267*, 264–270. [[CrossRef](#)]
67. Grosjean, T.; Saleh, S.S.; Suarez, M.A.; Ibrahim, I.A.; Piquerey, V.; Charraut, D.; Sandoz, P. Fiber microaxicons fabricated by a polishing technique for the generation of Bessel-like beams. *Appl. Opt.* **2007**, *46*, 8061–8067. [[CrossRef](#)]
68. Žukauskas, A.; Malinauskas, M.; Brasselet, E. Monolithic generators of pseudo-nondiffracting optical vortex beams at the microscale. *Appl. Phys. Lett.* **2013**, *103*, 181122. [[CrossRef](#)]
69. Chi, W.; George, N. Electronic imaging using a logarithmic sphere. *Opt. Lett.* **2001**, *26*, 875–877. [[CrossRef](#)]
70. Golub, I.; Chebbi, B.; Shaw, D.; Nowacki, D. Characterization of a refractive logarithmic axicon. *Opt. Lett.* **2010**, *35*, 2828–2830. [[CrossRef](#)]
71. Khonina, S.N.; Ustinov, A.V. Very compact focal spot in the near-field of the fractional axicon. *Opt. Commun.* **2017**, *391*, 24–29. [[CrossRef](#)]
72. Gorelick, S.; Paganin, D.M.; de Marco, A. Axilenses: Refractive micro-optical elements with arbitrary exponential profiles. *APL Photonics* **2020**, *5*, 106110. [[CrossRef](#)]
73. Sanchez-Padilla, B.; Žukauskas, A.; Aleksanyan, A.; Balčytis, A.; Malinauskas, M.; Juodkazis, S.; Brasselet, E. Wrinkled axicons: Shaping light from cusps. *Opt. Express* **2016**, *24*, 24075–24082. [[CrossRef](#)] [[PubMed](#)]
74. Khonina, S.N.; Krasnov, S.V.; Ustinov, A.V.; Degtyarev, S.A.; Porfirev, A.P.; Kuchmizhak, A.; Kudryashov, S.I. Refractive twisted microaxicons. *Opt. Lett.* **2020**, *45*, 1334–1337. [[CrossRef](#)] [[PubMed](#)]
75. Gonzalez-Acuña, R.G.; Guitiérrez-Vega, J.C. Generalization of the axicon shape: The gaxicon. *J. Opt. Soc. Am. A* **2018**, *35*, 1915–1918. [[CrossRef](#)]
76. Khonina, S.N.; Kazanskiy, N.L.; Khorin, P.A.; Butt, M.A. Modern Types of Axicons: New Functions and Applications. *Sensors* **2021**, *21*, 6690. [[CrossRef](#)]
77. Sokolov, A.L. Calculation of polarization aberrations by the method of polarization-wave matrices. *Opt. Spectrosc.* **2007**, *103*, 640–645. [[CrossRef](#)]
78. Khonina, S.N. Vortex beams with high-order cylindrical polarization: Features of focal distributions. *Appl. Phys. B* **2019**, *125*, 100. [[CrossRef](#)]
79. Kharitonov, S.I.; Khonina, S.N. Conversion of a conical wave with circular polarization into a vortex cylindrically polarized beam in a metal waveguide. *Comput. Opt.* **2018**, *42*, 197–211. [[CrossRef](#)]